Applied Thermal Engineering 190 (2021) 116826

Contents lists available at ScienceDirect

Applied Thermal Engineering

journal homepage: www.elsevier.com/locate/apthermeng

Experimental assessment of a thermoelectric subcooler included in a transcritical CO_2 refrigeration plant

P. Aranguren [a,b,*], D. Sánchez [c], A. Casi [a,b], R. Cabello [c], D. Astrain [a,b]

[a] Engineering Department Public University of Navarre, Campus de Arrosadia s/n, 31006 Pamplona, Spain
[b] Smart Cities Institute, 31006 Pamplona, Spain
[c] Department of Mechanical Engineering and Construction, Jaume I University, Campus de Riu Sec s/n, 12071 Castellón, Spain

ARTICLE INFO

Keywords:
CO_2
Thermoelectric subcooler
Subcooling
R744
Transcritical operation
COP

ABSTRACT

This study brings an experimental research that has tested a real transcritical CO_2 vapor compression cycle that includes a thermoelectric subcooler at the exit of the gas-cooler of the refrigeration plant. The aforementioned technology hybridization increases the COP of refrigeration systems as long as the subcooling system is properly designed and operated. The experimental facility studied has been tested under constant ambient conditions (30 °C and relative humidity of 55%) and maintaining the evaporating temperature at −10 °C; while the voltage supplied to the thermoelectric modules and the thermal resistances of the heat exchangers located at the thermoelectric subcooler have been experimentally modified. The voltage supplied to the fans located at these heat exchangers was modified implying thermal performance deviation of the heat exchangers and a variation on the power consumption of the cooling facility. The results show an experimental increase on the COP of 11.3% while the cooling capacity increases a 15.3% when the thermoelectric modules are supplied with 2 V and the fans with 9 V. Moreover, the importance of optimizing the voltage supplied to the thermoelectric modules and to the auxiliary consumption of the thermoelectric subcooler is addressed along this research.

1. Introduction

The International Institute of Refrigeration (IIR) stated that refrigeration and heating, ventilation and air conditioning (HVAC) systems are responsible for the emission of 2.61 Gt of CO_2, the 7.8% of the global Greenhouse gas emissions [1]. Due to this significant percentage, CO_2 refrigeration systems were rescued by Prof. Lorentzen in the nineties as a reasonable and technical possibility to replace artificial refrigerants in HVAC and refrigeration applications [2]. During the past years, the interest in Carbon dioxide (R744) as a refrigerant has increased due to its non-flammability, non-toxicity, easy availability, cheapness, environmentally friendliness, as a consequence of its zero Ozone Depletion Potential (ODP), negligible direct Global Warming Potential (GWP < 1) and favourable thermophysical properties. This natural refrigerant presents lower viscosity and higher latent heat, thermal conductivity, density, volumetric cooling capacity and specific heat than HFCs [3]. However, due to its low critical temperature (30.89 °C) refrigeration systems would work under transcritical operation as soon as the outdoor temperature exceeds a threshold, reaching high operating pressures that would negatively affect the coefficient of performance (COP) of these systems.

As a response to the low COPs of transcritical CO_2 cycles, several modifications to the basic single-stage refrigeration cycle have been introduced. Ejectors [4], expanders [5], internal heat exchangers [6], dedicated mechanical subcooling [7] or thermoelectric subcoolers [8] are some of the modifications suggested in the literature. In 2014 the IIR estimated that more than 1.5 billion domestic refrigeration systems and more than 55 million stand-alone systems for commercial refrigeration exist worldwide [9]. These small and medium-size refrigeration systems could benefit from the mentioned modifications, especially transcritical systems with CO_2, but in most of the cases the extra cost and complexity derived from the inclusion of these modifications would not compensate the COP increment of the refrigeration systems. Small to medium-size refrigeration systems need to incorporate subtle modifications and the increased complexity of operation has to be virtually imperceptible. Moreover, the modifications included need to have a reduced size and a low price in order to be considered.

Thermoelectric coolers are solid-state refrigerators that take advantage of the Peltier effect to pump heat [10]. These devices have been proved to be an option at those applications where the inherent advantages of thermoelectricity outperform other technologies.

* Corresponding author.
E-mail address: patricia.arangureng@unavarra.es (P. Aranguren).

https://doi.org/10.1016/j.applthermaleng.2021.116826
Received 17 September 2020; Received in revised form 3 March 2021; Accepted 4 March 2021
Available online 12 March 2021

Nomenclature

Definition	Units
α	Seebeck coefficient of a TEM V/K
C_p	Isobaric specific heat J/kgK
COP	Coefficient of performance
COP^{n-f}	Coefficient of performance without including the consumption of the fans
COP^{TEM}	TEM Coefficient of performance
COP^{TESC}	TESC Coefficient of performance
h_{eva}^{in}	Enthalpy at the inlet of the evaporator J/kg
h_{eva}^{out}	Enthalpy at the outlet of the evaporator J/kg
h_{TESC}^{in}	Enthalpy at the inlet of the TESC J/kg
h_{TESC}^{out}	Enthalpy at the outlet of the TESC J/kg
I_{hp}	Current supplied to heat plate A
I_{TEM}	Current supplied to TEMs A
K	Conductance of a TEM W/K
$\dot{m}_{CO2}$	CO_2 mass flow kg/s
$\dot{m}_{wg}$	Water-glycol mass flow kg/s
$\dot{Q}_c^{TEM}$	Cooling capacity of each TEM W
$\dot{Q}_h^{TEM}$	Heat rejection of each TEM W
$\dot{Q}_h^{TESC}$	Heat rejection of the TESC W
$\dot{Q}_o$	Cooling capacity of the cooling facility W
$\dot{Q}_o^{TESC}$	Cooling capacity of the TESC W
P_{gc}	Heat rejection pressure bar
r	Electric resistivity of a TEM Ω
R_c	Cold side heat exchanger thermal resistance K/W
R_{cond}	Conductive thermal resistance K/W
R_{conv}	Convective thermal resistance K/W
R_h	Hot side heat exchanger thermal resistance K/W
T_O	Evaporating temperature °C
T_{amb}	Ambient temperature°C
T_c	Cold reservoir temperature °C
T_c^{TEM}	TEM cold side temperature °C
T_h	Heat sink temperature °C
T_{fd}	Finned dissipator temperature °C
T_h^{TEM}	TEM hot side temperature °C
T_{wg}^{in}	Inlet temperature water-glycol mixture °C
T_{wg}^{out}	Outlet temperature water-glycol mixture °C
V_{fan}	Voltage supplied to fans V
V_{hp}	Voltage supplied to heat plate V
V_{TEM}	Voltage supplied to TEMs V
$\dot{W}_{com}$	Power consumed by the compressor W
$\dot{W}_{TESC}$	Power consumed by the TESC W
$\dot{W}_{fan}$	Power consumed by the fans W

Thermoelectric cooling is proved to work at Portable refrigerators [11], high-power LED cooling [12], portable atmospheric water generator [13], computer chip cooling [14], passenger cabin's parking refrigeration [15] and distillation systems [16], where the reliability, small size, modularity, easiness of control, absence of moving parts and lack of maintenance are crucial to choose thermoelectricity. A thermoelectric cooler is formed by thermoelectric modules (TEMs) and heat exchangers located on both sides of the modules in order to optimize their performance. The closer the hot side temperature of the TEM to the heat sink and the TEM cold side temperature to the cold reservoir the better these devices perform, hence, the heat exchangers located on both sides need to be carefully designed. The influence of the heat transfer area, thermal conductance and heat transfer mechanisms existing at the heat exchangers over the performance of the thermoelectric coolers is present along the literature [12,17,18]. Moreover, not only the heat exchangers, but also the voltage supplied to the TEMs has to be optimized, as the Joule effect generated inside the module by the input current plays a crucial role in the performance of the thermoelectric coolers [19,20]. Thus, when a thermoelectric cooler is designed, some parameters, such as the voltage supply, current, supply, heat exchangers and thermal contact resistances, need to be studied and optimized in order to optimize the performance of the system.

The idea of including thermoelectric subcooling into vapor compression refrigeration systems using transcritical CO_2 as their working fluid has been proposed by several authors with the aim of improving the performance of the cooling facilities. Radermacher et al. firstly proposed the idea in 2005 through an innovative patent [8]. Afterwards, Schoenfeld et al. proposed the hybridization of these two technologies through an experimental test bench that included 10 TEMs, an R-22 thermosyphon loop and an aluminium microchannel CO_2 heat exchanger, obtaining a COP improvement of the 5.2% and an increase on the cooling capacity of the 9.2% [21]. Further studies done by the same authors encountered COP improvements as high as 10% thanks to heat transfer and assembling optimization of the thermoelectric subcooler (TESC) [22]. Then, in 2013 Sarkar proposed a computational model obtaining a 25.6% improvement on the COP of the system and a 15.4% reduction on the optimum discharge pressure [23]. In 2015 Yazawa et al. obtained an increment of the 22.6% on the COP by a computational model simulating the refrigeration of a Data Center [24]. Subsequently. Dai et al. combined a TESC with an expander for transcritical CO_2 refrigeration cycles obtaining a simulated increase of the COP equal to the 37.8% [25]. In 2017 Jamali et al. proposed to integrate two-stage TEMs both in the gas-cooler and as a subcooler of a transcritical CO_2 refrigeration cycle to obtain improvements in the COP of 19% [26]. Astrain et al. proposed a computational study on the parameters of a TESC obtaining a maximum improvement of 24.12% on the COP [27]. In 2019 Liu et al. proposed the inclusion of a TESC and an ejector into a CO_2 vapor compression system, getting an improvement of 39.34% [28]. And finally, in 2020 Sanchez et al. experimentally obtained a 9.9% improvement on the COP of a transcritical CO_2 facility thanks to a TESC [29].

Since the first experimental approach to test the benefits of including thermoelectric subcooling into transcritical CO_2 refrigeration systems, many authors have computationally studied the benefits of the hybridization of these two technologies. Table 1 proves that this synergy turns out to be very beneficial, nevertheless, most of the studies do not include the effect of the heat exchangers located at the TESC, a crucial factor needed to be included if accurate results want to be obtained. Furthermore, the auxiliary consumption of the TESC is not included into the theoretical calculations, a very important aspect that has to be taken into account if the performance of the refrigeration facility wants to be optimized [30,31].

Therefore, the present research experimentally studies the benefits of including a thermoelectric subcooling system into a transcritical CO_2 vapor compression system. This study tests a real refrigeration facility that works under constant evaporating and ambient temperatures while the voltage supply to the TEMs and the thermal resistances of the heat exchangers of the TESC are experimentally varied to seek for the optimum performance point of the entire system. Along with the thermal resistances modification, the power consumption attributed to the auxiliary equipment is modified to accomplish the optimal system. Furthermore, the operation along the TESC is analysed, the temperatures of the CO_2, the temperatures of the sides of the TEMs and the COPs of the TESC are studied to obtain main conclusions about the

Table 1
Literature review of the inclusion of thermoelectric subcooling into transcritical CO_2 refrigeration systems.

Authors	Experimental (E)Simulation (S)	Included technologies	TESC studied parameters	ΔCOP(%)	$\Delta\dot{Q}_o$(%)	ΔP_{dis}(%)
Schoenfeld et al. [22]	E	TESC	10 TEM; CO_2 microchannel HX; R134a thermoshyphon	10%	13%	−0.32%
Sarkar et al. [23]	S	TESC	Current supply	25.6%	—	−15.4%
Yazawa et al. [24]	S	TESC	Subcooling temperature	22.6%	6%	−10%
Dai et al. [25]	S	TESC + expander	Subcooling temperature; TEM current supply	37.8%	—	−18%
Jamali et al. [26]	S	Two-stage TESC + TEG	TEM current supply; Thermocouples ratio	19%	—	−4%
Astrain et al. [27]	S	TESC	TEM number; Heat exchangers; TEM voltage supply	24.12%	33.27%	−6.9%
Liu et al. [28]	S	TESC + ejector	Subcooling temperature	39.34%	—	−8.01%
Sánchez et al. [29]	E	TESC	TEM voltage supply	9.9%	16%	−3.3 bar

performance of the TESC at this particular application.

2. Experimental setup

2.1. Refrigeration system

This section describes the configuration of a single-stage vapor compression system where a TESC has been included to study its influence on the COP of the entire refrigeration system. The refrigeration system has been designed for CO_2 transcritical operation with a cooling capacity of approximately 280 W and a two-stage expansion process in order to control the heat rejection pressure and the useful superheating at the evaporator. Fig. 1 presents the schematic of the experimental setup. A hermetic reciprocating compressor with a cubic capacity of 1.1 cm^3 (B) compresses the low pressure vapor that exits the evaporator (A) to a high-pressure level set by an electronic valve (F). The high pressure and temperature refrigerant that exits the compressor passes through a coalescing filter (C) which removes any presence of PAG lubricating oil, making sure that this oil returns to the compressor for its proper operation. The refrigerant cools down as it circulates through the finned gas-cooler (D) which uses a fan to make the ambient air circulate through its coil, with a transfer area of 0.27 m^2. Afterwards, the refrigerant is further cooled down at the TESC (E) formed by four copper blocks that accommodate eight thermoelectric modules (TEMs). Once subcooled, the refrigerant is expanded firstly by the electronic expansion valve (F) and secondly by another electronic expansion valve that controls useful superheating (H). Both expansion valves are connected by an accumulation tank of 3.7 L (G) that ensures the presence of liquid at the second valve. Finally, the outlet of the latter valve is connected to a brazed-plate evaporator (A) where the refrigerant is evaporated using a mixture of water/ethylene-glycol (51%/49% by mass) and a heat transfer area of 0.576 m^2.

Fig. 2 depicts the entire refrigerating plant where all the elements have been insulated with foam with an average thermal conductivity of 0.0036 W/mK according to ISO 13787. The thermoelectric subcooling system, which is further described in the following section, can be found at the front of Fig. 2.

2.2. Thermoelectric subcooler (TESC)

The TESC is intended to further decrease the temperature of the CO_2 after the gas-cooler. The TEMs are the core of the TESC, they are solid-state refrigerators that thanks to the Peltier effect absorb heat from the CO_2 when provided with electrical power [10]. The operation of thermoelectric coolers greatly depends on the temperature on both sides of the TEMs. The minimum difference possible is the one in between the heat source and the heat sink. Consequently, heat exchangers need to be located on both sides of the TEMs to obtain the minimum difference in temperature possible.

The used TEMs are Marlow Industries RC12-8-01*L* [32]. These bismuth-telluride modules have 127 thermocouples, each semiconductor presents a length of 0.13 cm and a cross-sectional area of 0.14 × 0.14 cm^2. The total size of the modules is 40 × 40 cm^2 and the ZT provided by the manufacturer is 0.73 at a cold side temperature of 27 °C [32].

As the working pressure of the CO_2 at the exit of the gas-cooler is very high the design of the heat exchanger to be located on the CO_2 side needs to be rigid enough not only not to break but also not to be deformed in order to minimize the contact thermal resistances. These thermal resistances need to be reduced to a minimum to ensure optimal performance by the subcooling system, and flatness of the heat exchangers is crucial for optimal contact between the TEMs and the heat exchangers

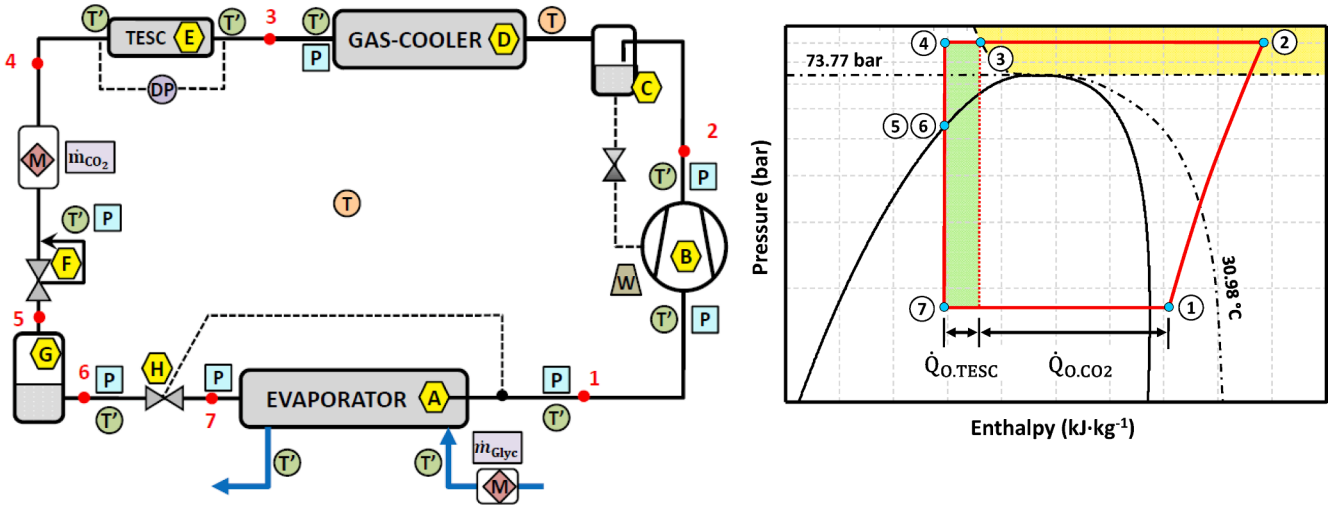

Fig. 1. a) Schematic of the refrigeration facility. b) P-h diagram of the system.

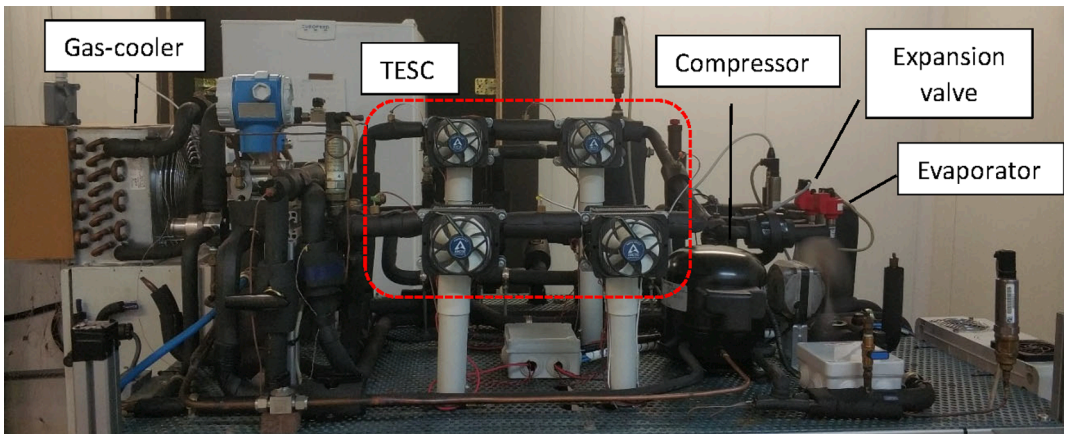

Fig. 2. Refrigeration facility.

[21,22]. Consequently, on the CO_2 side, copper blocks with machined channels for CO_2 circulation are located, while finned dissipators are placed on the hot sides of the TEMs. Considering the cooling capacity of the base refrigeration systems, four copper blocks in series are installed at the exit of the gas-cooler with a total of eight TEMs and similar number of finned dissipators, as the schematic of Fig. 3 shows.

Each copper block has external dimensions of $74 \times 60 \times 10$ mm^3 and includes two TEMs, one on each side. The CO_2 flows through the interior of the blocks thanks to a drilled path, which presents an internal heat exchange area of 0.0037 m2 per block thanks to a 3 mm tube that meanders thought the compact block. In order to maximize the performance of the subcooler, finned heat exchangers provided with fans have been located on the hot side of the TEMs. Each finned dissipator is provided with 35 fins with a height, spacing and thickness of 28 mm, 1.5 mm and 2 mm, respectively. Moreover, a fan with a nominal consumption of 1.56 W ensures that the air circulates through the fins, as the detail of Fig. 4 shows. In order to reduce the contact thermal resistances all the flat surfaces of the heat exchanger where the TEMs were located were sanded and polished and the mounting process was done very carefully with four bolts per block. Moreover, a torque wrench was used to provide the manufacture's recommended torque and thermal grease with a conductivity of 5 W/mK was included on each interface between the TEMs and the heat exchangers. Finally, the pipes and the copper blocks were insulated using foam with an average conductivity of 0.0036 W/mK.

The TESC system if fully monitored to assess its operation. Fig. 3 includes the position of all the measuring devices. Five immersion temperature probes, one at each entry of the four copper blocks and one at the exit of the TESC can be found. Besides, on each copper block two temperature probes are present, one on each side of the TEM measuring T_H^{TEMi} and T_C^{TEMi}, respectively. Likewise, a pressure difference probe between the entry and the exit of the TESC and two multimeters that measure the DC voltages and currents supplied to the TEMs and the fans can be found.

2.3. Measurement instrumentation and acquisition system

The entire refrigeration system, including the TESC, is fully monitored through a data acquisition system (DAQ) formed by several modules. Figs. 1 and 4 present the location of the instrumentation used to measure the operation of the system. There can be found 23 T-type temperature probes (13 immersion probes (T') and 10 superficial probes (T)); 7 pressure probes (P); 1 differential pressure probe (DP); 2 Coriolis mass flow meters (M) and 2 digital wattmeters (W). Table 2 includes the main characteristics of the used measurement probes.

The information of the DAQ system is recorded by a personal computer. The post processing uses Excel, Matlab, RefProp v.9.1 and SecCool v.1.33 software. Data are recorded each 5 s during a minimum acquisition of 20 min once the permanent stage has been reached.

2.4. Experimental methodology

During all tests the refrigeration system has been tested under Climatic Class IV conditions following ISO 23953-2:2015 ($T_{amb} = 30$ °C and $RH_{amb} = 55\%$). Moreover, the evaporating temperature was maintained to −10 °C, the useful superheating was set to 4 K and the gas-cooler pressure was maintained to 83.3 bar. This discharge pressure was chosen as it is the optimum pressure for the mentioned system when the TESC system is included [29]. Meanwhile, the voltage supplied to the TEMs as well as the voltage supplied to fans that provide forced convection to the finned dissipators located on the hot side of the TEMs were varied.

The cooling capacity of the system can be obtained by Eq. (1) where the mass flow of the CO_2 is measured by a Coriolis mass flow meter ($\dot{m}_{CO2}$) and the enthalpies at the entry and exit of the evaporator are calculated with RefProp v.9.1 using the temperatures and pressures at

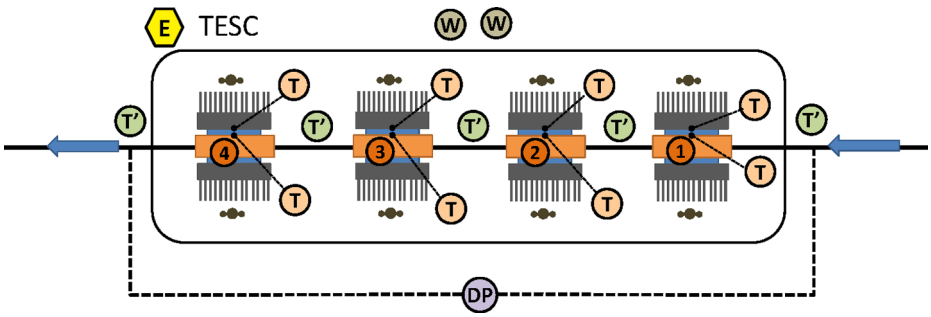

Fig. 3. Schematic of the thermoelectric subcooler.

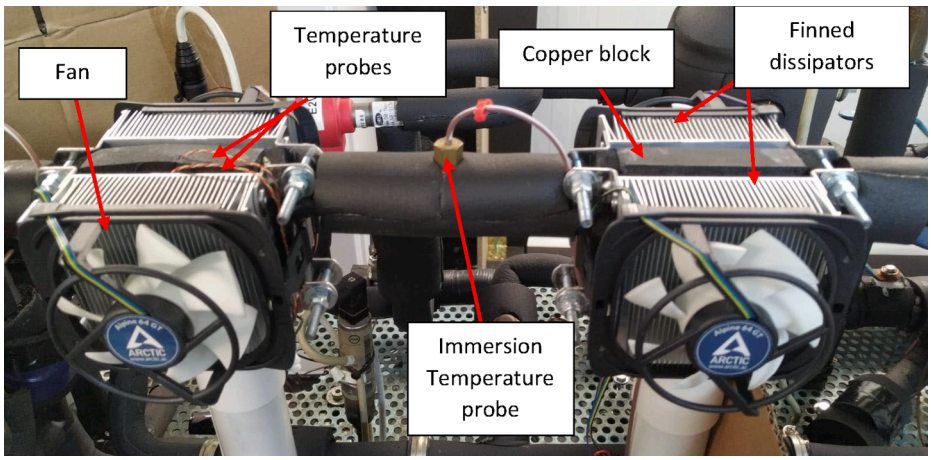

Fig. 4. Detail of the thermoelectric subcooling system.

Table 2
Main characteristics of the measurement probes.

Measured value	Measuring device	Sensibility	Accuracy
Temperature	T-type thermocouple	0.01 °C	±0.5 °C
Pressure (HP)	Pressure gauge	0.01 bar	±0.6% full scale
Pressure (MP)	Pressure gauge	0.01 bar	±0.6% full scale
Pressure (LP)	Pressure gauge	0.01 bar	±0.6% full scale
Pressure	Differential pressure	0.01 bar	±0.5% full scale
CO_2 mass flow rate	Coriolis mass flow meter	0.01 kg/h	±0.5% of reading
Water/glycol mass flow rate	Coriolis mass flow meter	0.01 kg/h	±0.5% of reading
Power consumption	Network analyser	0.01 W	±0.5% of reading
DC voltage	Digital multimeter	0.01 V	±0.05% of reading
DC current	Digital multimeter	0.01 A	±0.2% of reading

each point ($h_{eva}^{out}, h_{eva}^{in}$).

$$\dot{Q}_o = \dot{m}_{CO2}(h_{eva}^{out} - h_{eva}^{in}) \quad (1)$$

$$\dot{Q}_o = \dot{m}_{wg} C_p (T_{wg}^{in} - T_{wg}^{out}) \quad (2)$$

The cooling capacity of the refrigeration facility can also be obtained through the heat absorbed from the secondary fluid of the evaporator, a mixture of water and glycol. The water/glycol circulates through the brazed-plate evaporator and controls the evaporating temperature thanks to a heating resistor controlled by a PID system. The temperatures of the water-glycol mixture at the entry and exit of the evaporator are measured ($T_{wg}^{in}, T_{wg}^{out}$), the mass flow is measured using a Coriolis mass flow meter ($\dot{m}_{wg}$) and the specific heat is obtained introducing the percentage of the water-glycol mixture into SecCool v.1.33 software (C_p). Fig. 5 plots the cooling capacity obtained using Eq. (2) versus that obtained by Eq. (1) for all the tests developed (different voltages supplied to the TEMs and different voltages to the fans). As it can be seen, the discrepancies between both results are within a ±10%, being most of them between the ±5% range.

The COP of the entire refrigeration system is calculated using Eq. (3). This equation includes the power consumed by the compressor and the power consumption by the TESC (Eq. (4)). The latter equation includes not only the power consumed by the TEMs, but also the power consumed by the fans of the finned dissipators located on the hot side of the TEMs.

$$COP = \frac{\dot{Q}_o}{\dot{W}_{com} + \dot{W}_{TESC}} \quad (3)$$

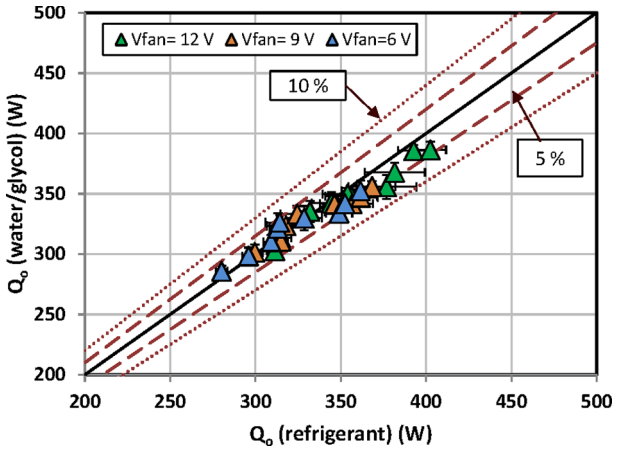

Fig. 5. Data validation with the measuring data at the evaporator.

$$\dot{W}_{TESC} = V_{TEM} I_{TEM} + V_{fan} I_{fan} \quad (4)$$

$$COP^{TEM} = \frac{\dot{Q}_o^{TESC}}{V_{TEM} I_{TEM}} \quad (5)$$

$$COP^{TESC} = \frac{\dot{Q}_o^{TESC}}{\dot{W}_{TESC}} \quad (6)$$

$$\dot{Q}_o^{TESC} = \dot{m}_{CO2}(h_{TESC}^{in} - h_{TESC}^{out}) \quad (7)$$

Likewise, the coefficients of performance of the TEM and TESC, Eqs. (5) and (6), respectively, are calculated for the different scenarios studied. The COP of the TESC includes the consumption of the fans located on the hot side of the TEMs while the COP of the TEM does not. In both cases, the cooling capacity of the TESC has been calculated using Eq. (7), where the measured CO_2 mass flow is multiplied by the difference of enthalpies between the inlet and the outlet of the TESC.

Each test has been recorded during the steady operation of the refrigeration facility and data have been logged each 5 s for a period always bigger than 20 min. For this period of time, the results show the average value of each measurement and the error bars represent the standard deviation of each variable along each period of time.

3. Experimental analysis when modifying the voltage supplied to the tems

The performance of the TESC determines the benefits of including this system into the transcritical CO_2 cycle. The voltage supplied to the thermoelectric modules, as well as the voltage supplied to the fans included into the finned dissipators determine the performance of the TESC, and consequently they need to be studied to seek for the optimum working point. Section 3 analyses the influence of modifying the voltage supplied to the TEMs, while Section 4 analysis the influence of modifying the voltage supplied to the fans involved in heat rejection of the TESC.

3.1. Analysis of the refrigeration facility

In order to analyse the benefits of including the TESC, firstly the base cycle (without TESC) was studied at different discharge pressures. The optimum working conditions corresponds to a pressure of 86.6 bar, a COP of 1.03 and a cooling capacity of 289.0 W for ambient temperature of 30 °C, evaporating temperature of −10 °C and useful superheating of 4 K [29]. Table 3 includes this data. The incorporation of the described TESC system to the CO_2 base cycle decreases the pressure 3.3 bar, obtaining an optimum gas cooler pressure of 83.3 bar [29].

Fig. 6 presents the COP and the cooling capacity of the refrigeration system for both the base cycle and that including the TESC as a function of the voltage supplied to the TEMs. It can be concluded that low voltage supplies improve the performance of the cycle, while high voltage supplies (higher than 4 V) worsen the performance of the facility obtaining lower COP than the optimum COP of the base cycle. The COP of the system including the TESC presents and optimum when the TEMs are supplied with 2 V, obtaining a 9.9% increment on the COP compared to the base cycle.

Likewise, the cooling capacity increment is very remarkable, at maximum TEM voltage supply the system is able to increase a 33.7% its cooling capacity, however, this operating point would not be adequate, as the COP of the refrigeration facility drastically worsens with respect to the base cycle one. Within the range where adding the TESC is interesting, the increase of cooling capacity presents a lineal tendency, a fact that is very beneficial to control the refrigeration facility by only adjusting the voltage supplied to the TEMs.

Fig. 7 shows the cooling capacity, COP and power consumption increments regarding the base cycle at the region where including the TESC is beneficial. The reason why the COP decreases once the supplied voltage to the TEMs is higher than 2 V is due to the significant increase of the consumed power by the TESC, as Fig. 8 presents. Besides, Fig. 8 present a 3% decrease on the compressor work due to the reduction on the high side optimum pressure when the TESC is added.

3.2. TESC operation analysis

Eqs. (8)–(10) determine the operation of a thermoelectric refrigerator in terms of the hot and cold temperatures of each TEM, the current supplied to each TEM and the parameters that define the thermoelectric modules [33]. The properties that define a TEM are: Seebeck coefficient, α (V/K), thermal conductance, K (W/K), and the electric resistivity, r (Ω). These parameters are dependent on temperature, but as the working temperatures are not going to be very different, it can be deduced that the temperatures of the cold and hot sides of the modules define the

Table 3
Base cycle optimum operating conditions [29].

Optimum operating conditions base cycle (T_{amb} : 30°C; T_o = −10°C)	
COP	1.034
Cooling capacity (W)	289.0
Heat dissipation pressure (bar)	86.6

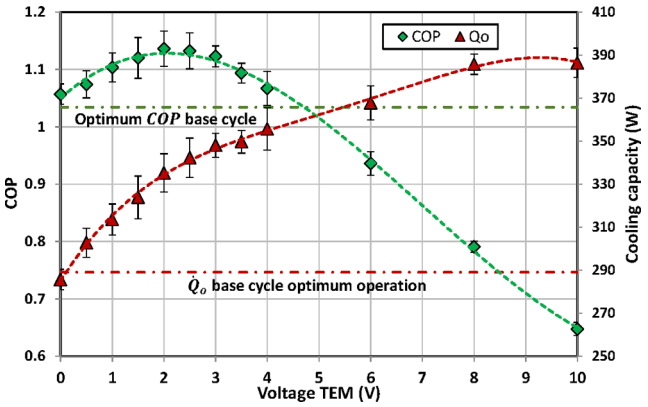

Fig. 6. COP and cooling capacity of the refrigeration facility including the TESC (T_{amb} : 30°C; T_o : −10°C; P_{gc} : 83.3*bar*; V_{fan} : 12*V*).

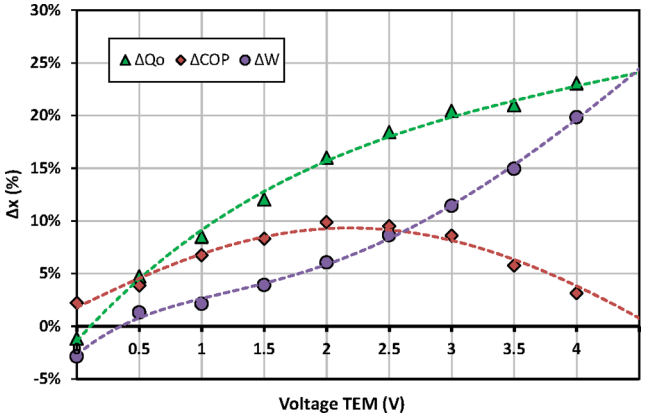

Fig. 7. Increments regarding the optimum working operation of the base cycle of the cooling capacity, COP and power consumption as a function of the voltage supplied to the TEM (T_{amb} : 30°C; T_o : −10°C; P_{gc} : 83.3*bar*; V_{fan} : 12*V*).

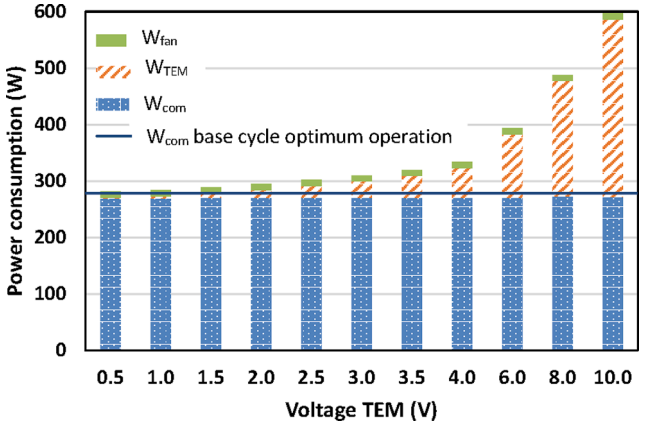

Fig. 8. Power consumption of the compressor, thermoelectric modules and fans of the TESC (T_{amb} : 30°C; T_o : −10°C; P_{gc} : 83.3*bar*; V_{fan} : 12*V*).

heat extracted from the CO_2 ($\dot{Q}_o^{TESC}$)and also the heat released to the ambient ($\dot{Q}_h^{TESC}$). Thus, at this particular application the performance of the TESC is greatly defined by the temperatures of the sides of the TEM, where the cold side is always referred to the side where the heat is going to be extracted from (CO_2) and the hot side to the side where the heat is released to (ambient). Likewise, these temperatures are determined by the thermal resistances ($R_c and R_h$) of the heat exchangers located on both

sides of the TEMs, while these values depend on the conduction and convection phenomena that take place at the copper blocks for the cold side heat exchanger and at the finned dissipators for the hot side of the TEMs.

$$\dot{Q}_o^{TESC} = \sum \dot{Q}_c^{TEMi} = \sum \left(\alpha I_{TEMi} T_c^{TEMi} - \frac{1}{2} I_{TEMi}^2 r - K\left(T_h^{TEMi} - T_c^{TEMi}\right) \right) \quad (8)$$

$$\dot{Q}_h^{TESC} = \sum \dot{Q}_h^{TEMi} = \sum \left(\alpha I_{TEMi} T_h^{TEMi} + \frac{1}{2} I_{TEMi}^2 r - K\left(T_h^{TEMi} - T_c^{TEMi}\right) \right) \quad (9)$$

$$\dot{Q}_c^{TEMi} = \frac{T_c - T_c^{TEMi}}{R_{ci}}; R_{ci} = f(R_{conv}, R_{cond}) \quad (10)$$

$$\dot{Q}_h^{TEMi} = \frac{T_h^{TEMi} - T_h}{R_{hi}}; R_{hi} = f(R_{conv}, R_{cond}) \quad (11)$$

$$\dot{W}_{TEM} = \sum \dot{W}_{TEMi} = \sum \left(\dot{Q}_h^{TEMi} - \dot{Q}_c^{TEMi} \right) \approx \alpha I_{TEMi} \left(T_h^{TEMi} - T_c^{TEMi}\right) + I_{TEMi}^2 r \quad (12)$$

3.2.1. Temperature of the CO_2

Fig. 9 depicts the temperature of the CO_2 as it flows along the TESC. The x axis determines the position along the TESC, 0 stands for the entry, 1 determines the outlet of block 1, 2 that of block 2, 3 that of block 3 and four is the exit of block 4, the outlet of the TESC. Position 0 corresponds to the exit of the gas-cooler, and therefore it represents the approach of the gas-cooler, approximately 3 K along the experiments conducted. The maximum subcooling degree obtained corresponds to 18.8 °C, however this subcooling entails a big power consumption by the TEMs and consequently could not be the optimal working point.

3.2.2. Temperature of the hot and cold sides of the TEMs

The study of the cold and hot side temperatures is very important to understand the behaviour of the TESC. The cold side temperatures along the TESC vary to a greater extent than that of the hot side, as Fig. 10 presents. This is because the temperature of the cold reservoir decreases as the refrigerant circulates along the TESC while the temperature of the heat sink is constant, 30 °C. The temperature difference between the two sides at each TEM gets bigger as the voltage supplied to the TESC increases. A higher power supplied to the TEM implies higher heat power extracted from the refrigerant and consequently a higher heat power emitted to the ambient, as Eqs. (8) and (9) show. Thus, the temperatures of the hot and cold sides move away from the temperatures of the heat sink and cold reservoir, respectively, as Fig. 10 depicts.

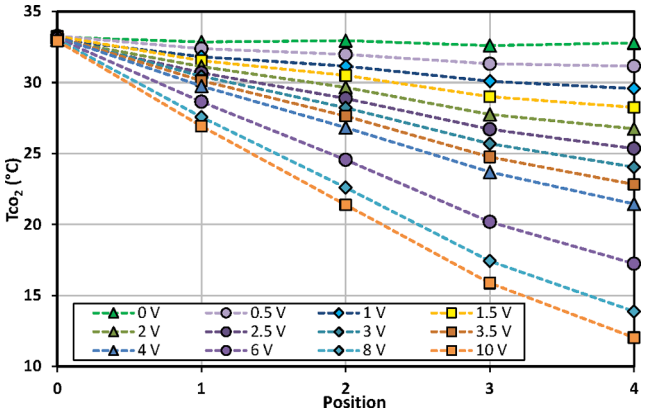

Fig. 9. Temperature of the CO_2 at the outlet of each TESC block depending on the voltage supplied to the TEMs (T_{amb} : 30°C; T_o : −10°C; P_{gc} : 83.3*bar*; V_{fan} : 12*V*).

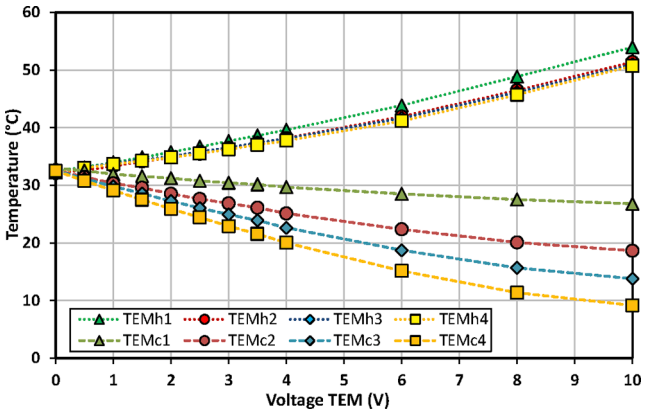

Fig. 10. Hot and cold side temperatures of the different blocks of the TESC as a function of the voltage supplied (T_{amb} : 30°C; T_o : −10°C; P_{gc} : 83.3*bar*; V_{fan} : 12*V*).

3.2.3. Cooling capacity

Fig. 11 depicts the cooling capacity provided by each block of the TESC, and the total cooling capacity. The first block is subtracting a bigger amount of power than the rest as its temperature difference in between faces is lower, as Fig. 7 shows. Furthermore, the temperature and pressure of the CO_2 at the first block locates its operation very near the pseudocritical region, and hence, the heat transfer within this block is better than that at the other blocks. The percentages of cooling capacity obtained by each block are kept more or less constant when the voltage supplied to the TEMs varies. As an example, when the voltage supplied to the TESC is 10 V, the first block is subtracting the 39% of the total cooling capacity, while the second, third and fourth blocks are subtracting the 25; 21 and 14%, respectively. The maximum cooling capacity that the designed TESC can provide to the system is 137.3 W. This cooling capacity is directly reflected into the capacity of the entire refrigeration facility, being very beneficial for the refrigeration system at pull-down processes.

3.2.4. COP

Fig. 12 presents both the COP of the TEM and the COP of the TESC. The calculation of the first one only includes the consumption of the TEMs (Eq. (5)) while the second one includes the consumption of the fans (Eq. (6)). It is important to note that the values of the ordinate axes are very different, the left ordinate axis (COP^{TEM}) is one order or magnitude bigger than the right one (COP^{TESC}). This is due to the adding of the consumption of the fans, which drastically reduces the COP

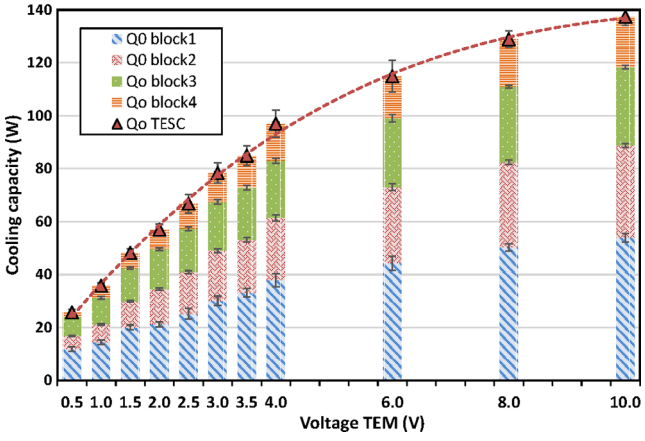

Fig. 11. Cooling capacity of each block of the TESC and total cooling capacity as a function of the voltage supplied (T_{amb} : 30°C; T_o : −10°C; P_{gc} : 83.3*bar*; V_{fan} : 12*V*).

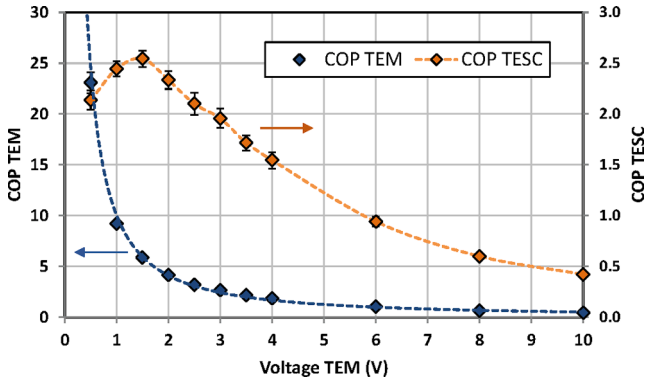

Fig. 12. COPs of the TESC (T_{amb} : 30°C; T_o : −10°C; P_{gc} : 83.3*bar*; V_{fan} : 12*V*).

values.

When the TEMs are supplied with low voltages, their COP is high, nevertheless, as the voltage increases the COP drastically decreases. When the voltage supplied to the TEMs increases, the cooling capacity increases (Eq. (8)), however, the power consumption of the modules increases to a greater extent (Eq. (12)) resulting into smaller COPs.

The COP of the TESC presents an optimum point at 1.5 V. For low voltages, the cooling power increase obtained when increasing the voltage supplied to the TEMs is higher than the increment on the total consumption (fans and TEMs). Nevertheless, when the voltage supplied to the TEMs is higher than 1.5 V the increase on total consumption is higher than the cooling capacity increase, and thus the COP of the TESC starts decreasing.

3.2.5. Pressure drop

Regarding the pressure drop introduced by the TESC, the maximum drop that the refrigerant suffers when circulating through the TESC is 151 mbar, an insignificant value compared to the high working pressure, 83.3 bar. In this particular case, the pressure drop of including thermoelectric subcooling into this transcritical CO_2 vapor compression system is negligible, however, if subcooling wants to be added to vapor compression systems working with other refrigerants, such as isobutene or propane, this pressure drop would be needed to be taken into account.

4. Experimental analysis when modifying the voltage supplied to the fans of the finned dissipators

The consumption of the TESC is obtained adding the consumption of the TEMs and the consumption of the fans of the hot side finned dissipators. Hence, the consumption of the fans need to be also optimized in order to optimize the performance of the refrigeration system. Moreover, the fans determine the thermal resistance of the finned dissipators, thus the temperatures of the TEMs are defined by the fans, and consequently their performance greatly depends on them.

To obtain the dependence of the thermal resistance of the dissipators on the voltage supplied to the fans, a small test bench was designed and built. A finned dissipator was sandwiched with a steel plate having in between a heat plate with the size of a TEM (40 × 40 mm^2). Moreover, the system was properly insulated in order not to let heat dissipation to the rear side or the side covers. Likewise, a temperature probe on the finned dissipator (T_{fd}) and two more probes to measure the ambient temperature (T_{amb}) were located while the heat to be dissipated was supplied to the heat plate by a DC power source ($\dot{Q} = V_{hp}I_{hp}$). Eq. (13) was used to determine the thermal resistances, dependent on the voltage supplied to the fan while independent on the heat flux to dissipate [34].

$$R_h = \frac{T_{fd} - T_{amb}}{V_{hp}I_{hp}} \tag{13}$$

The thermal resistance of the finned dissipators decreases when the voltage supplied to the fans increases. As Fig. 13 shows, a reduction of the 40% on the thermal resistance is produced when increasing the voltage supplied to the fans from 6 to 12 V, an increase of the 300% on the fan power consumption. Reducing the thermal resistance of the finned dissipators is crucial for the performance of the TESC, as the hot side temperatures would decrease, and hence the COP of the TESC would increase (Eqs. (10)–(12)). Nonetheless, this reduction implies a great increase on the consumption of the TESC, a very negative impact on the performance of the whole system.

To determine the optimum performance of the entire refrigeration system, three voltages were applied to the fans 6, 9 and 12 V.

4.1. Analysis of the refrigeration facility

It can be seen how the COP of the system finds an optimum at 2 V applied to the TEMs for the cases of 12 and 9 V supplied to the fans (Figs. 6 and 14), while when the fans are supplied with 6 V the optimum of the entire system appears when the voltage of the TEMs equals 1.5 V. When the fans are supplied with less power, the thermal resistances of the finned dissipators increase, and hence, the optimum performance of the refrigeration system is better when smaller voltages are supplied to the TEMs.

The optimum COP value of 1.15 for the entire cooling capacity is obtained when 9 V and 2 V are supplied to the fans and TEMs, respectively. Consequently, increments of the 11.3% on the COP with respect to the optimal performance of the base system (without TESC) are obtained when the TESC system is included and its performance is optimized. At this optimum scenario, not only the COP is optimized, but also the cooling capacity increases a 15.3% in comparison with the base cycle.

Fig. 15 includes the power consumption of the main elements of the cooling system, highlighting the strong impact of modifying the consumption of the fans located at the hot side heat exchangers of the TESC. The latter figure shows how the consumption of the fans is of the same magnitude as the consumption of the TEMS, especially for low voltage supplies, where the optimum lays. Thus, it is very important to also optimize the power consumption of the fan in order to obtain the maximum COP.

4.2. TESC operation analysis

4.2.1. Temperature of CO_2

The operation of the TESC is determined by the heat exchangers located on both sides of the TEMs. The higher the voltage supplied to the fans (better thermal resistances of the heat exchangers) the higher the subcooling achieved by the TESC, as Fig. 16 presents.

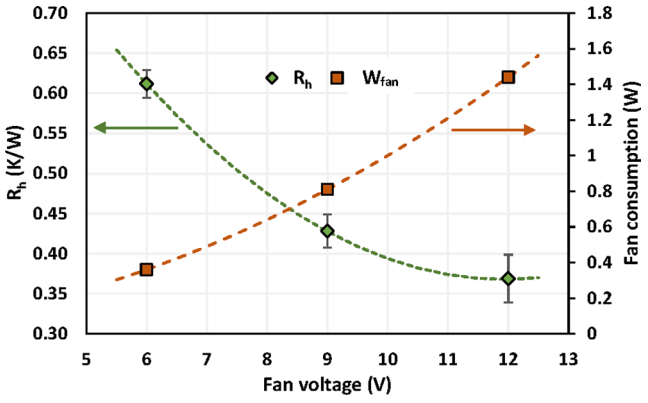

Fig. 13. Thermal resistance of the finned dissipators and their power consumption as a function of their voltage supplied.

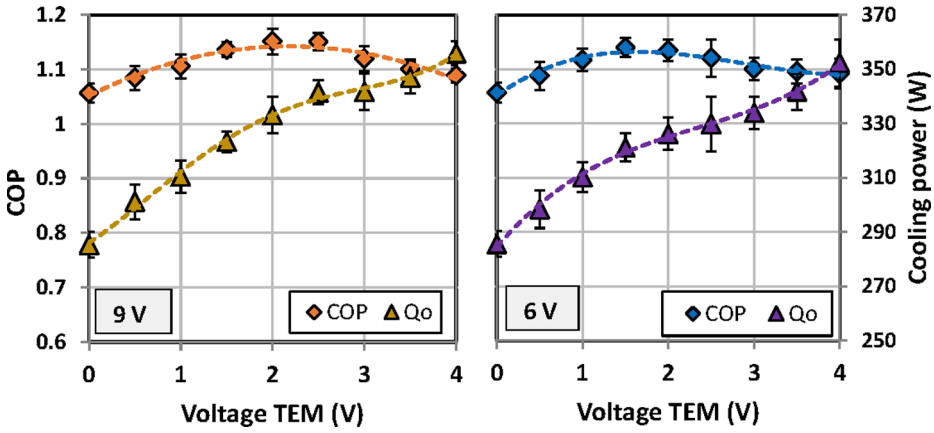

Fig. 14. Operation of the refrigeration system when modifying the voltage supplied to the fans (T_{amb} : 30°C; T_o : −10°C; P_{gc} : 83.3*bar*).

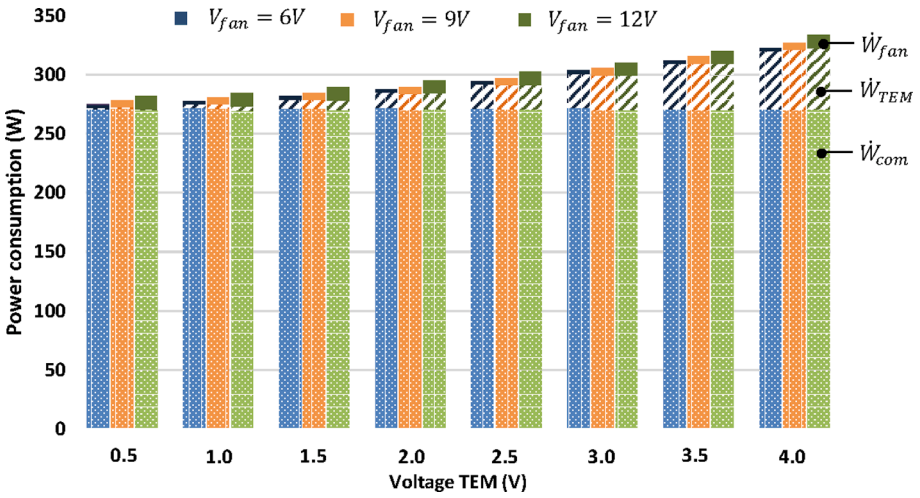

Fig. 15. Power consumption of the compressor, TEM and fans for the different voltage supplied to the fans of the fin dissipators (T_{amb} : 30°C; T_o : −10°C; P_{gc} : 83.3*bar*).

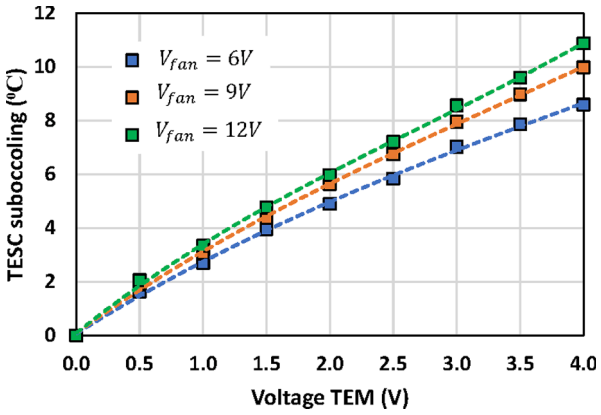

Fig. 16. TESC subcooling for different voltage supplied to the fans of the finned dissipators (T_{amb} : 30°C; T_o : −10°C; P_{gc} : 83.3*bar*).

4.2.2. *Temperature of the hot and cold sides of the TEMs*

Fig. 17 presents the temperatures of the hot and cold sides of the TEMs located at the first block when the voltages supplied to TEMs and to fans are modified. Reducing the voltage supplied to the fans provokes an increase on the thermal resistance of the dissipators of the hot side of the TEMs, and consequently, the temperature of the hot side increases, as Fig. 17 shows. Nevertheless, the cold side temperature is barely modified when the voltage of the fans vary, hence, the differences of temperature represented reflect the variation of the hot side temperature. The same tendencies could be observed at the other blocks of the TESC.

4.2.3. *Cooling capacity*

The better the thermal resistance of the finned dissipators (higher voltage supplied to the fans) the higher the cooling capacity achieved by the TESC, as Fig. 18 presents. Nevertheless, the higher the voltage supply to the fans the higher the power consumption by the TESC, consequently, the COP of the TESC will present an optimum.

4.2.4. *COP*

The higher the temperature difference between the sides of the TEMs the lower the COP of the TEMs, however, the tendency of the COP of the TESC is completely different, as Fig. 19 presents. The COP of the TESC includes the consumption of the auxiliary equipment, the fans, hence as the voltage supplied to the fans decreases the COP^{TESC} increases, as the reduction of power consumed by the fans is more important than the reduction of cooling capacity achieved. However, the optimum points for the COP^{TESC} at each voltage supplied to the fans do not correspond with the optimum working points of the entire refrigeration facility.

4.2.5. *Pressure drop*

The pressure drop suffered by the CO_2 when 6 and 9 V are supplied to the fans are similar for the case of 12 V, as the temperature change of the

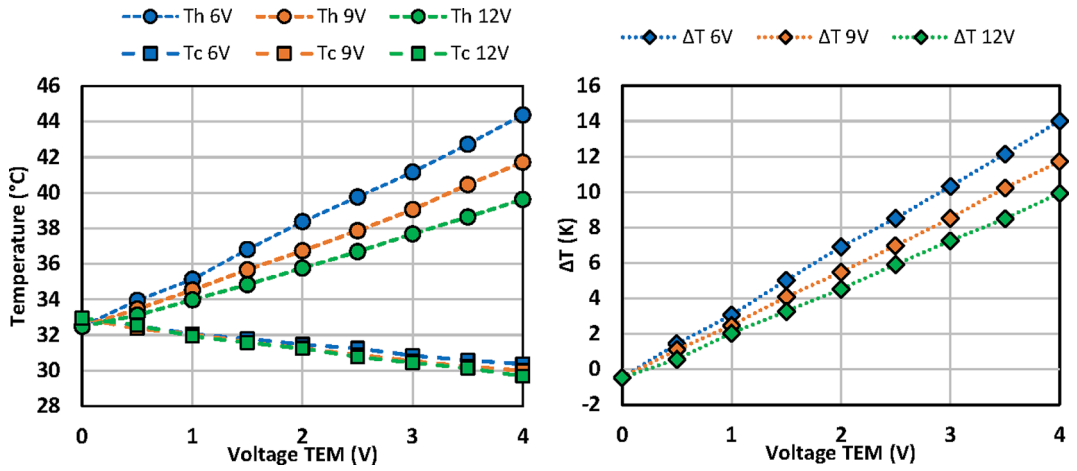

Fig. 17. Temperatures of the hot and cold sides of the TEMs of the first block when the voltages supplied to the TEMs and fans are modified (T_{amb} : 30°C; T_o : −10°C; P_{gc} : 83.3*bar*).

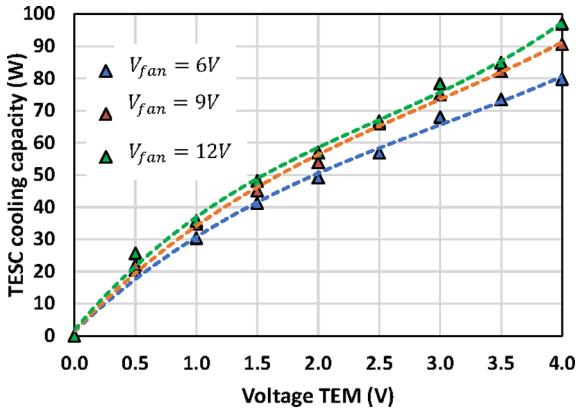

Fig. 18. TESC cooling capacity for different voltage supply to the fans of the heat exchangers (T_{amb} : 30°C; T_o : −10°C; P_{gc} : 83.3*bar*).

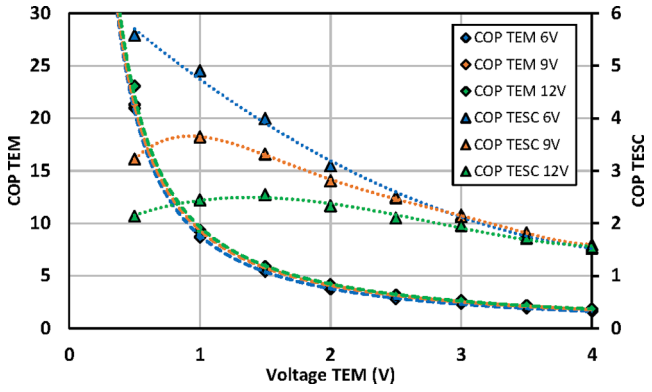

Fig. 19. COPs of the refrigeration system when the voltage supplied to TEM and fans are modified (T_{amb} : 30°C; T_o : −10°C; P_{gc} : 83.3*bar*).

CO_2 are not significant to modify the pressure losses suffered when circulating through the copper blocks.

5. Summary of the experimental results

Table 4 includes the most important parameters of the optimum working points of the refrigeration facility when different fan voltage supplies are tested. The effect of increasing the power consumption of the fans can be observed, the COP of the TEMs increase as well as the subcooling and the cooling capacities as a result of a smaller temperature difference between the hot and cold sides of the TEMs. Nevertheless, the COP of the TESC decreases if the consumption of the fan increases, as a result of a significant increase on the consumption of the fans. The latter leads to the optimum working point of the entire cooling capacity when 9 V are supplied to the fans, which provides a 11.3% improvement on the COP with respect to the base cycle. At this point, the COP of the TEMs is 4.02 and that of the TESC is 2.81. Moreover, the cooling capacity provided by the TESC at this optimum point is 53.9 W and the subcooling degree 5.6 K.

The increments present in Table 4 have been obtained throughout Eq. (14).

$$\Delta X = \frac{X_{TESC} - X_{basecycle}}{X_{basecycle}} 100(\%) \tag{14}$$

Finally, the TESC system could be located at the entrance of the air stream of the gas-cooler, taking advantage of the already existing mass flow of air in order to obtain the forced convection at the finned dissipators located on the hot side of the TESC. The air would circulate first through the TESC system and afterwards through the gas-cooler. In this case, the gas-cooler operation would not be harmed, as the temperature of the air would not increase drastically, and consequently, the consumption of the fans of the TESC could be eliminated. Table 4 includes the COP of the system if the consumption of the fans is eliminated $\left(COP^{n-f} = \frac{\dot{Q}_o}{W_{com}+V_{TEM}I_{TEM}}\right)$ as a result of locating the TESC at the air stream of the gas-cooler. At this scenario the optimum point is obtained when 12 V are supplied to the fans. This optimal point has 4.17 and 2.33 as its COP of the TEM and COP of the TESC, respectively, a subcooling degree of 6.0 K and a cooling capacity of 56.9 W. Moreover, the improvement of COP thanks to including the TESC into the system ascends to a 14% obtaining a COP of 1.18. Additionally, at this optimal point the cooling capacity would increase a 16%, a very important advantage that the inclusion of the TESC also provides into the refrigeration system.

Both optimal scenarios present increments on the COP of the refrigeration facility of 11.3 and 14.1%, respectively, very important improvements achieved when a TESC is included into a vapor compression system. Besides, the cooling capacity of the refrigeration facility for these two scenarios, obtains increments of 15.3 and 16%, being very beneficial for the performance of the entire system. Thus, it could be concluded that the inclusion of thermoelectric subcooling systems into a vapor compression system working with CO_2 under

Table 4
Optimum working points for different supplied voltages to the fans of the finned dissipators. (T_{amb} : 30°C; T_o : −10°C).

	TESC						Refrigeration facility					
	V_{fan}	V_{TEM}	COP^{TEM}	COP^{TESC}	SUB	$\dot{Q}_o{}^{TESC}$	COP		$\dot{Q}_o$(W)		COP^{n-f}	
	(V)	(V)			(K)	(W)	Value	ΔCOP	Value	$\Delta\dot{Q}_0$	Value	ΔCOP
Base cycle $P_{gc} = 86.6bar$	–						1.034	0%	289.0	0%	1.034	0%
TESC $P_{gc} = 83.3bar$	6	1.5	5.41	3.99	4.1	41.2	1.140	10.2%	321.2	11.1%	1.150	11.2%
	9	2.0	4.02	2.81	5.6	53.9	1.151	11.3%	333.3	15.3%	1.175	13.6%
	12	2.0	4.17	2.33	6.0	56.9	1.136	9.9%	335.3	16.0%	1.180	14.1%

transcritical conditions could be very beneficial as not only does the performance of the system improve, but also the cooling capacity increases. Moreover, the price, reliability, easiness of operation and scarce maintenance of the TESC system supports the hybridization of these two technologies to foster the optimization of middle size cooling facilities.

6. Conclusions

This work has implemented an experimental vapor compression refrigeration system, working under CO_2 transcritical conditions and including a thermoelectric subcooler at the exit of the gas-cooler. The inclusion of the TESC into the refrigeration system does not imply an increment on the complexity of the entire system neither on the maintenance operation, due to the simplicity, modularity, easiness of operation and control, reliability, and absence of refrigerants. The voltage supplies to the thermoelectric modules and to the fans of the heat exchangers located on the hot side of the thermoelectric subcooler are modified in order to obtain the optimal working point for the entire refrigeration system.

The optimum working point of the facility is obtained when the discharge pressure is 83.3 bar, the voltage supplied to the thermoelectric modules 2 V and the voltage supplied to the fans is 9 V. At this working point the COP of the entire system is 1.15 (11.3% improvement with respect to the base cycle) and the cooling capacity increments a 15.3%. Moreover, the COP of the thermoelectric modules is 4.02 and that of the subcooling system is 2.81, the cooling capacity provided by the TESC is roughly 54 W and the subcooling degree 5.6 K.

The inclusion of a thermoelectric subcooler at the exit of the gas-cooler of a vapor compression refrigeration system working with transcritical CO_2 is very beneficial for its performance. Thus, the further work of this research is to perform energetic studies for stand-alone commercial refrigeration systems including thermoelectric subcooling to affirm this inclusion is beneficial at real working operation.

Declaration of Competing Interest

The authors declare that they have no known competing financial interests or personal relationships that could have appeared to influence the work reported in this paper.

Acknowledgements

The authors would like to acknowledge the support of the Spanish Ministry of Science, Innovation and Universities, and European Regional Development Fund, for the funding under the RTI2018-093501-B-C21 and RTI2018-093501-B-C22 research projects.

Appendix A. Supplementary data

Supplementary data to this article can be found online at https://doi.org/10.1016/j.applthermaleng.2021.116826.

References

[1] IIR, The impact of the refrigeration sector on climate change, Informat. Note Refrig. Technol. (2017).
[2] G. Lorentzen, The use of natural refrigerants: a complete solution to the CFC/HCFC predicament, Int. J. Refrig 18 (1995) 190–197, https://doi.org/10.1016/0140-7007(94)00001-E.
[3] Y.T. Ge, S.A. Tassou, Thermodynamic analysis of transcritical CO2 booster refrigeration systems in supermarket, Energy Convers Manag. 52 (2011) 1868–1875, https://doi.org/10.1016/j.enconman.2010.11.015.
[4] S. Li, J. Yan, Z. Liu, Y. Yao, X. Li, N. Wen, et al., Optimization on crucial ejector geometries in a multi-evaporator refrigeration system for tropical region refrigerated trucks, Energy 189 (2019), 116347, https://doi.org/10.1016/j.energy.2019.116347.
[5] D.M. Robinson, E.A. Groll, Efficiencies of transcritical CO2 cycles with and without an expansion turbine, Int. J. Refrig. 21 (1998) 577–589, https://doi.org/10.1016/S0140-7007(98)00024-3.
[6] E. Torrella, D. Sánchez, R. Llopis, R. Cabello, Energetic evaluation of an internal heat exchanger in a CO2 transcritical refrigeration plant using experimental data, Int. J. Refrig. 34 (2011) 40–49, https://doi.org/10.1016/J.IJREFRIG.2010.07.006.
[7] D. Sánchez, J. Catalán-Gil, R. Cabello, D. Calleja-Anta, R. Llopis, L. Nebot-Andrés, Experimental Analysis and Optimization of an R744 Transcritical Cycle Working with a Mechanical Subcooling System, Energies 13 (2020) 3204, https://doi.org/10.3390/en13123204.
[8] R. Radermacher, B. Yang, Innovative thermoelectric- assisted vapor-compression refrigeration systems. US PS-2005-076, 2005.
[9] ADEME, AFCE, UNICLIMA, EReIE, Cemafroid. Alternative to high GWP in refrigeration and air-conditioning applications, 2013.
[10] D.M. Rowe, CRC Handbook of Thermoelectrics, New York 16 (1995) 1251–1256, https://doi.org/10.1016/S0960-1481(98)00512-6.
[11] T. Gong, Y. Wu, L. Gao, L. Zhang, J. Li, T. Ming, Thermo-mechanical analysis on a compact thermoelectric cooler, Energy 172 (2019) 1211–1224, https://doi.org/10.1016/j.energy.2019.02.014.
[12] X. Lin, S. Mo, B. Mo, L. Jia, Y. Chen, Z. Cheng, Thermal management of high-power LED based on thermoelectric cooler and nanofluid-cooled microchannel heat sink, Appl. Therm. Eng. 172 (2020), 115165, https://doi.org/10.1016/j.applthermaleng.2020.115165.
[13] W. He, P. Yu, Z. Hu, S. Lv, M. Qin, C. Yu, Experimental study and performance analysis of a portable atmospheric water generator, Energies 13 (2019), https://doi.org/10.3390/en13010073.
[14] D. Liu, Y. Cai, F.Y. Zhao, Optimal design of thermoelectric cooling system integrated heat pipes for electric devices, Energy 128 (2017) 403–413, https://doi.org/10.1016/j.energy.2017.03.120.
[15] X. Ma, G. Tan, S. Wang, D. Zhou, Y. Ding, Z. Ma, et al., Passenger cabin's parking cooling system based on TEC and air conditioning condensate water. SAE Tech Pap 2019; 2019-April, https://doi.org/10.4271/2019-01-1066.
[16] H. Al-Madhhachi, G. Min, Effective use of thermal energy at both hot and cold side of thermoelectric module for developing efficient thermoelectric water distillation system, Energy Convers Manag. 133 (2017) 14–19, https://doi.org/10.1016/J.ENCONMAN.2016.11.055.
[17] L. Zhu, H. Tan, J. Yu, Analysis on optimal heat exchanger size of thermoelectric cooler for electronic cooling applications, Energy Convers Manag. 76 (2013) 685–690, https://doi.org/10.1016/j.enconman.2013.08.014.
[18] D. Astrain, P. Aranguren, A. Martínez, A. Rodríguez, M.G. Pérez, A comparative study of different heat exchange systems in a thermoelectric refrigerator and their influence on the efficiency, Appl. Therm. Eng. (2016;103.), https://doi.org/10.1016/j.applthermaleng.2016.04.132.
[19] T. Gong, L. Gao, Y. Wu, L. Zhang, S. Yin, J. Li, et al., Numerical simulation on a compact thermoelectric cooler for the optimized design, Appl. Therm. Eng. 146 (2019) 815–825, https://doi.org/10.1016/J.APPLTHERMALENG.2018.10.047.
[20] A. Elarusi, A. Attar, H. Lee, Optimal Design of a Thermoelectric Cooling/Heating System for Car Seat Climate Control (CSCC), J. Electron. Mater. 46 (2017) 1984–1995, https://doi.org/10.1007/s11664-016-5043-y.
[21] J. Schoenfeld, J. Muehlbauer, Y. Hwang, R. Radermacher, Integration of a Thermoelectric Subcooler into a Carbon Dioxide Transcritical Vapor Compression Cycle Refrigeration System, Refrig. Air Cond. (2008) 1–8.
[22] J.M. Schoenfeld, Integration of a thermoelectric subcooler into a carbon dioxide transcritical vapor compression cycle refrigeration system, 2008.

[23] J. Sarkar, S. Bhattacharyya, Performance optimization of transcritical CO2 refrigeration cycle with thermoelectric subcooler, Int. J. Energy Res. 33 (2013) 121–128, https://doi.org/10.1002/er.

[24] K. Yazawa, S. Dharkar, O. Kurtulus, E.A. Groll, Optimum design for thermoelectric in a sub-cooled trans-critical CO2 heat pump for data center cooling. Annu. IEEE Semicond. Therm Meas. Manag. Symp. 2015; 2015-April: 19–24. https://doi.org/10.1109/SEMI-THERM.2015.7100133.

[25] B. Dai, S. Liu, K. Zhu, Z. Sun, Y. Ma, Thermodynamic performance evaluation of transcritical carbon dioxide refrigeration cycle integrated with thermoelectric subcooler and expander, Energy 122 (2017) 787–800, https://doi.org/10.1016/j.energy.2017.01.029.

[26] S. Jamali, M. Yari, F. Mohammadkhani, Performance improvement of a transcritical CO2 refrigeration cycle using two-stage thermoelectric modules in sub-cooler and gas cooler, Int. J. Refrig. 74 (2017) 103–113, https://doi.org/10.1016/j.ijrefrig.2016.10.007.

[27] D. Astrain, A. Merino, L. Catalán, P. Aranguren, M. Araiz, D. Sánchez, et al., Improvements in the cooling capacity and the COP of a transcritical CO2 refrigeration plant operating with a thermoelectric subcooling system, Appl. Therm. Eng. 155 (2019) 110–122, https://doi.org/10.1016/J.APPLTHERMALENG.2019.03.123.

[28] X. Liu, R. Fu, Z. Wang, L. Lin, Z. Sun, X. Li, Thermodynamic analysis of transcritical CO2 refrigeration cycle integrated with thermoelectric subcooler and ejector, Energy Convers Manag. 188 (2019) 354–365, https://doi.org/10.1016/j.enconman.2019.02.088.

[29] D. Sanchez, P. Aranguren, A. Casi, R. Cabello, R. Llopis, Experimental enhancement of a CO2 transcritical refrigerating plant including thermoelectric subcooling, Int. J. Refrig. 120 (2020) 178–187.

[30] P. Aranguren, M. Araiz, D. Astrain, Auxiliary consumption: A necessary energy that affects thermoelectric generation, Appl. Therm. Eng. 141 (2018) 990–999, https://doi.org/10.1016/j.applthermaleng.2018.06.042.

[31] P. Aranguren, D. Astrain, Thermoelectric Power Generation Optimization by Thermal Design Means. Thermoelectr. power Gener. A look trends, Technol. Intech (2016) 437–460, https://doi.org/10.5772/65849.

[32] Marlow Industries Inc. RC12-8-01L 2020. https://ii-vi.com/wp-content/uploads/2020/07/TG12-8.pdf (accessed February 5, 2021).

[33] P. Aranguren, S. DiazDeGarayo, A. Martínez, M. Araiz, D. Astrain, Heat pipes thermal performance for a reversible thermoelectric cooler-heat pump for a nZEB, Energy Build. 187 (2019) 163–172, https://doi.org/10.1016/j.enbuild.2019.01.039.

[34] P. Aranguren, D. Astrain, M.G. Pérez, Computational and experimental study of a complete heat dissipation system using water as heat carrier placed on a thermoelectric generator, Energy (2014).